Thin Solid Films 645 (2018) 424–430

Contents lists available at ScienceDirect

Thin Solid Films

journal homepage: www.elsevier.com/locate/tsf

Thin film growth of delafossite β-$NaFeO_2$ on a ZnO layer by pulsed laser deposition

Ioanna Bakaimi[a,b,*], Evie L. Papadopoulou[a,1], Georgios Kenanakis[a], Emmanouel Spanakis[c], Alexandros Lappas[a]

[a] Institute of Electronic Structure and Laser, Foundation for Research and Technology - Hellas, Heraklion 71110, Greece
[b] Department of Physics, University of Crete, Heraklion 71003, Greece
[c] Department of Materials Science and Technology, University of Crete, Heraklion 71003, Greece

ARTICLE INFO

Keywords:
Delafossites
Thin films
Pulsed laser deposition
Sodium iron ferrites
β-$NaFeO_2$

ABSTRACT

Despite the fact there is a plethora of magnetic delafossite compounds in the bulk polycrystalline phase, so far, only a few of them have been fabricated as thin films. The challenges in the fabrication of delafossite thin films are imposed by the phase purity and stability of the composition related with the preparation conditions. Here we report the growth of a new delafossite thin film, a sodium iron oxide of the β-$NaFeO_2$ phase, grown on a ZnO seed layer by pulsed laser deposition, using as target a single phase polycrystalline powder of β-$NaFeO_2$. The purity of the thin films has been verified with X-ray diffraction, Scanning electron and Atomic Force Microscopy as well as Fourier Transform Infrared Spectroscopy. The crucial parameter for the growth of the thin films has been the partial oxygen pressure, as the β-$NaFeO_2$ is obtained at 2 Pa. Applying higher or lower pressures resulted in the formation the hematite and maghemite iron oxides as secondary phases, as indicated by X-ray diffraction patterns. SEM and AFM studies confirm a good two dimensional growth for the pure phase β-$NaFeO_2$, whereas FT-IR measurements revealed characteristic β-$NaFeO_2$ bands.

1. Introduction

Delafossite compounds of the structure ABO_2 where A is copper, sodium, silver or an alkali-nonmagnetic cation and B is a trivalent magnetic ion have been of intense research interest over the last two decades [1]. The triangular lattice topology of the B magnetic cation directly influences several properties of delafossites, including the geometric magnetic frustration [2] and the magnetoelectric phenomenon [3]. Moreover, a wide range of structural modifications, can be designed into the crystal structure simply by changing the A-site with soft chemistry methods, such as intercalation [4,5] or deintercalation. The availability of having multiple ways to manipulate the properties of delafossites makes them an attractive material for numerous technological applications such as their use as cathode materials in batteries [6,7], p-type transparent conducting oxides [8–10], thermoelectrical materials [11] and gas sensors [12].

Additionally well-known delafossite compounds such as the $AgFeO_2$, [13] and$_2$ $CuFeO_2$ and $CuFe_{0.5}V_{0.5}O_2$ [14], $CuCrO_2$, [15] as well asthe triangular lattice antiferromagnets $ACrO_2$ [16] (A: Cu, Ag, Li or Na) have proven to possess multiferroic and magnetoelectric properties. However, due to various limitations [17,18] related with the mutually exclusive nature of the magnetic order in conjunction to the appearance of electric polarization, only a few compounds exhibit room temperature multiferroicity such as the $BiFeO_3$ [19] and the nanostructures $BaTiO_3$ and $CoFe_2O_4$ [20]. Recently, studies on single crystals of β-$NaFeO_2$, a room temperature weak ferromagnet, [21] revealed the coexistence of polarization and magnetic order at the same temperature, placing it as one of the very few existing room temperature multiferroics [22]. Studies of multiferroic thin film systems have shown significant enhancement of the magnetization, polarization and coupling properties when compared with their counterparts in bulk phases [23,24].

Lately, considerable interest has been directed towards the preparation of delafossite thin films [25–30], using as starting materials their bulk ceramic phases. One of the main challenges in the preparation of the delafossite oxide powders by high temperature solid state reaction is to obtain a single pure phase material. Many of the delafossite materials with a noble metal on the A site decompose before the reaction occurs [31]. Moreover, a significant number of them possess polymorphs, which are characterized by chemical structures with

* Corresponding author at: Department of Chemistry, University of Southampton, Southampton SO 171BJ, UK.
E-mail address: I.Bakaimi@soton.ac.uk (I. Bakaimi).
[1] Current address: Smart Materials, Istituto Italiano di Tecnologia, via Morego 30, 16163 Genoa, Italy.

https://doi.org/10.1016/j.tsf.2017.11.022
Received 20 June 2017; Received in revised form 7 November 2017; Accepted 14 November 2017
Available online 15 November 2017

energetic proximity, (as it happens for example in the case of $NaMnO_2$ [32] and $NaAlO_2$ [33] compounds), so each polymorph requires very precise preparation conditions. Since $NaFeO_2$ oxides can be found in three polymorphs, namely the α-$NaFeO_2$, β-$NaFeO_2$ and γ-$NaFeO_2$ [33,34] one easily realizes the constrains entailed in the preparation and the proper preservation of the β-$NaFeO_2$ oxides. Moreover, the β-phase is moisture sensitive, which induces another challenge when handling and storing this compound. Analogously, many parameters need to be taken into account when preparing a delafossite thin film deposition, such as the selection of the proper substrate, the temperature of its annealing and –what has been proven to be of outmost importance - the partial oxygen pressure applied during the pulsed laser deposition (PLD) growth.

Although numerous delafossite compounds have been reported as polycrystalline bulk materials, considerably less have been fabricated as thin films. The majority of these refer to Cu based oxides, such as the $CuFeO_2$, the $CuCrO_2$, $CuAlO_2$ and the $CuGaO_2$ obtained by pulsed laser deposition [8,31,35,36], radio frequency (RF) [9,25,37] or direct current (DC) [38] sputtering and sol gel based methods [10,29,39,40]. More recently Ag based oxides have been synthesized by combinatorial magnetron sputtering [41]. The challenges to overcome for making good quality delafossite thin films are related with the use of proper substrates for each deposited system, the control of the chemical composition ratio over a wide range of temperature and pressures. These factors contribute in the application of strict preparation conditions for obtaining a pure and stable phase thin film.

In this work we propose a simple approach for the growth of pure β-$NaFeO_2$ thin film, on a ZnO layer by pulsed laser deposition, introducing a novelty with wide range of prospects on the delafossite magnetic thin films and their possible applications. To the best of our knowledge it is the first time that the synthesis of a sodium iron oxide thin film is being reported, and opens up new directions in its broader use in applications.

2. Experimental section

2.1. Preparation of polycrystalline powders

$NaFeO_2$ oxides form three polymorphs [34]: α-$NaFeO_2$, β-$NaFeO_2$ and γ-$NaFeO_2$ in which the β- and γ-polymorphs have closely related structures [42]. Therefore the conditions of preparation were carefully selected as to avoid metastable phases from one polymorph to another or the appearance of secondary phases of various iron oxides. Stable and pure polycrystalline powders of β-$NaFeO_2$ were synthesized by slight modification on the synthetic protocol of the solid state reaction as reported earlier by Takeda et al. [34] Na_2CO_3 (Aldrich, 99,5 + %) and α-Fe_2O_3 (Alfa Aesar, 99%) were mixed, grounded and pressed into pellets (Ø12 mm at 0.5 ton for 5 min). The reddish pellet obtained was heated with a constant rate of 2.5 °C/min starting from room temperature and up to 850 °C under continuous oxygen flow. A 5% excess of Na_2CO_3 was added in the first grinding to compensate for the loss of sodium. After aging at 850 °C for 24 h the sample was quenched to room temperature, under O_2 atmosphere. The final product had brown color and was stored in Ar-filled MBRAUN anaerobic glove-box, since the β-$NaFeO_2$ was found to decompose in an oxidizing environment. After having exposed the sample in air for a total of 12 h the pellet's color turns into the reddish color of hematite α-Fe_2O_3, which was used as a starting material. X-ray diffraction revealed additional Bragg peaks attributed to hematite, verifying the moisture sensitive nature of the β-$NaFeO_2$ phase.

2.2. Preparation of β-$NaFeO_2$ thin films

Thin films of pure β-$NaFeO_2$ were grown on ZnO thin layers, by conventional pulsed laser deposition (PLD) under constant oxygen flow, using the aforementioned β-$NaFeO_2$ powders. A KrF excimer laser (Lambda Physik, $\lambda = 248$ nm, $\tau = 34$ ns pulse duration, 600 mJ/pulse maximum) was used for the ablation, delivering pulses at a repetition rate of 10 Hz. The beam was incident at an angle of 45° with respect to the rotating target and was focused by spherical lens to yield the required energy density in order to grow each of the desired films. The spot size was approximately 3.3 mm^2. The base pressure prior to deposition was better than 10^{-3} Pa. First, a ZnO seed layer was deposited on UV-graded fused silica (1 × 1 cm^2) placed parallel to the target at a distance of 4 cm following a previous work [43]. During deposition, 4000 pulses were delivered, while the partial O_2 pressure was 5×10^{-2} Pa the substrate temperature 300 °C, and laser beam fluence was 1.5 J/cm^2. Subsequently, the β-$NaFeO_2$ was grown on the ZnO seed layer. In this case, the partial O_2 pressure was in the range of 10–10^{-2} Pa the substrate temperature was 650 °C and the laser fluence was 3 J/cm^2 and 4000 pulses were delivered to the substrate. Prior any deposition the target was cleaned with ca.500 pulses, before the plume was allowed to reach the substrate.

After deposition, the samples were cooled to room temperature at the same oxidizing environment. The thickness of the films was measured by Scanning Electron Microscopy SEM at different positions, and was found to be quite uniform, with average values ranging from 130 nm to 150 nm. X-ray diffraction patterns (XRD), and Fourier Transform-Infrared spectroscopy (FT-IR) confirmed that the above experimental protocol resulted in a phase-pure β-$NaFeO_2$ thin film.

2.3. X-ray powder and thin film diffractograms

X-ray powder diffraction (XRPD) experiments were carried out on a Rigaku D/MAX-2000H rotating Cu anode diffractometer ($\lambda = 1.5406$ Å) on a θ/2θ mode with a step of 0.02°.

2.4. Scanning Electron Microscopy (SEM) and Atomic Force Microscopy (AFM) experiments

The morphology of the surfaces was examined by a field emission scanning electron microscope (FESEMJEOL 7000). Atomic Force Microscopy (AFM) surface topographies were taken using a Nanonics SPM1000 microscope, equipped with c-Si cantilever tips, driven in intermittent contact mode. The corresponding images were analyzed with the free WSxM software [44].

2.5. FT-IR experiments

Fourier Transform infrared spectroscopy (FT-IR) experiments were carried out with a Bruker IFS 66v/S spectrometer equipped with a broad band KBr detector and a room temperature broad band triglycine sulfate (DTGS) detector, in reflection mode using a Bruker A513/Q specular reflectance accessory at quasi-normal incidence of 13°. Interferograms were collected at 2 cm^{-1} resolution (32 scans), apodized with a Blackman-Harris function, and Fourier transformed with two levels of zero filling to yield spectra encoded at 2 cm^{-1} intervals. Prior to scanning the samples, a background gold mirror was recorded, and each sample spectrum was obtained by automatic subtraction of it.

3. Results and discussion

An example of the typical delafossite structure is represented by the low temperature rhombohedral (R3m) structure of the α-$NFeO_2$ oxide shown in Fig. 1(a). α-$NFeO_2$ consists of hexagonal FeO_2 layers of edge sharing FeO_6 octahedra separated by a layer of Na atoms. β-$NaFeO_2$ unlike any other member of the delafossite family adopts a wurtzite like structure presented in Fig. 1(b). This is the high temperature modification of the $NaFeO_2$, which is the orthorhombic (Pn21a) β-$NaFeO_2$ phase. In the β-$NaFeO_2$ the Fe^{3+} ions are in the centers of oxygen tetrahedral entities. The FeO_4 tetrahedra share corners in an ordered wurtzite arrangement whereas the sodium ions (yellow atoms in Fig. 1)

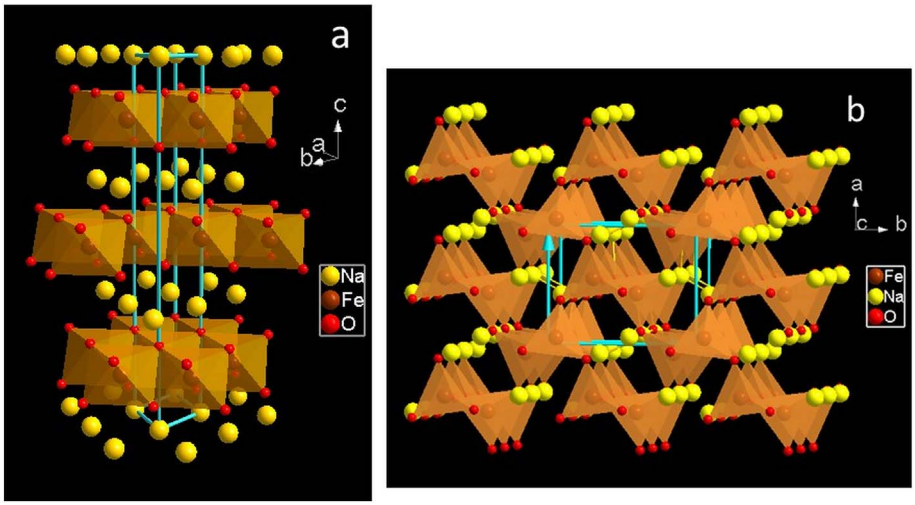

Fig. 1. Schematic representation of the crystal structures of the $NaFeO_2$ oxides the: α-$NaFeO_2$ (a) and the β-$NaFeO_2$ (b): iron, sodium and oxygen atoms are represented with the brown, yellow and red spheres, respectively. Cell edges are represented by the turquoise lines. In the β-$NaFeO_2$ phase, tetrahedra of FeO_4 share corners in an ordered wurtzite arrangement whereas the sodium ions occupy tetrahedral sites in the framework cavities. (ICSD 27117). (For interpretation of the references to color in this figure legend, the reader is referred to the web version of this article.)

occupy tetrahedral sites in the framework cavities.

To check the purity of the polycrystalline target, X-ray diffractograms have been obtained and analyzed using the FULLPROF suite [45] with a Le Bail method as shown in Fig. 2. The fit resulted in the following cell parameters: Pna21, a = 5.68(1) Å, b = 7.15(2) Å, c = 5.39(1) Å, α = 90°, β = 90°, γ = 90°, with good agreement factors (χ^2 = 7.65, R (Bragg) = 8.034%, R (F^2) = 5.37%) showing a satisfactory correspondence to the crystal structure parameters reported in the literature [46]. Since the characterization of the bulk β-$NaFeO_2$ revealed a single phase material, the next step was the fabrication of a thin film. The ZnO layer was chosen as a suitable substrate for the growth of β-$NaFeO_2$ since both of them crystallize in the orthorhombic space group with the characteristic wurtzite structure [47]. A comparison of the X-ray diffractograms from the single phase β-$NaFeO_2$ thin films and those obtained from the polycrystalline target is presented in Fig. 3(a) and (b). The first Bragg peaks of the target, namely those who correspond to the (110) and (011) reflections at 19.99° and 20.68°, respectively, are also observed in the X-ray diffraction pattern of the thin film. In addition, the (002) at 33.3° and (210) at 33.96°, which are the reflections with the strongest intensity, are common to the powder and the thin film, as it can be seen in Fig. 3. Although the delafossite

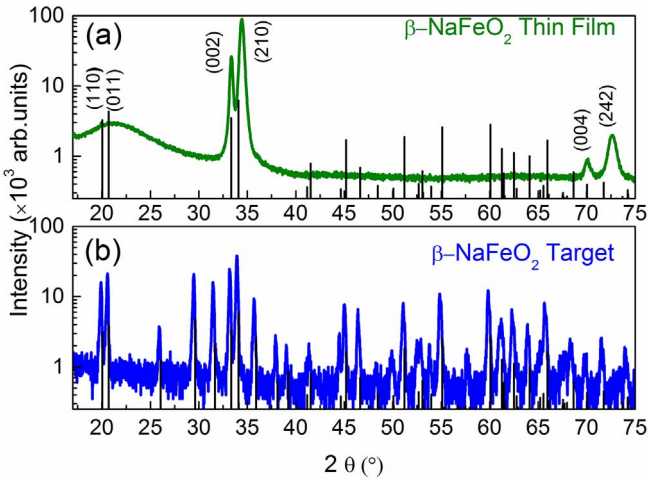

Fig. 3. X-ray diffraction patterns of the β-$NaFeO_2$ in a thin film form (a) and the corresponding polycrystalline target (b). The expected Bragg reflections in the orthorhombic cell (Pna21) are indicated with the black tick marks on both panels (a) and (b).

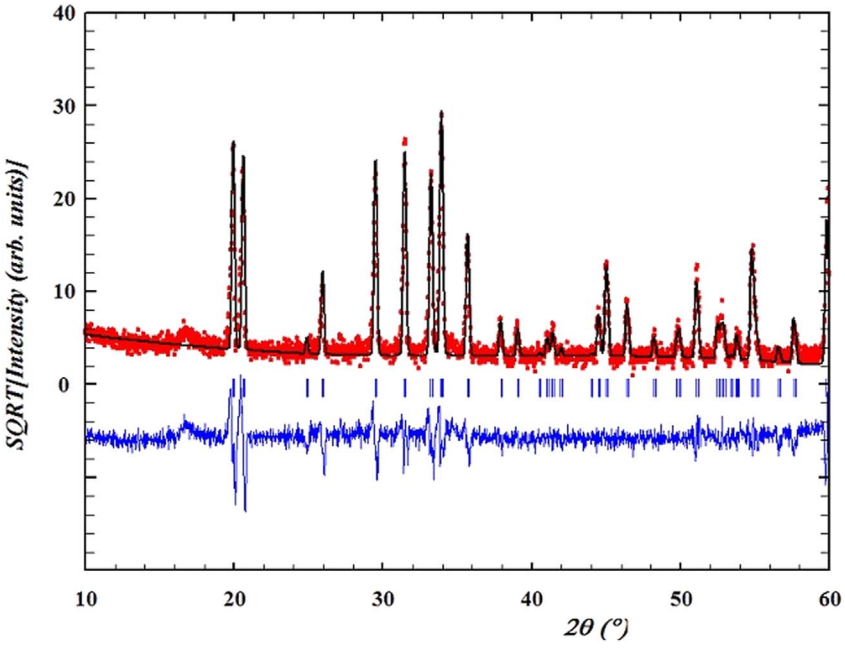

Fig. 2. Le Bail fit obtained for the orthorhombic cell (Pna21) of the X-ray diffraction data for the β-$NaFeO_2$ pollycrystalline target. The blue tick marks show the expected Bragg peak reflection positions, the red points and black line represent the observed and the calculated profile, respectively, whereas the blue line is the difference among them. (For interpretation of the references to color in this figure legend, the reader is referred to the web version of this article.)

Table 1
PLD experimental conditions for the growth of the β-$NaFeO_2$ thin films showing the appearance of iron oxides as secondary phases in various partial oxygen pressures.

Target temperature (°C)	Oxygen pressure (Pa)	Secondary phases
650	2×10^{1}	α-Fe_2O_3 (Hematite) and γ-Fe_2O_3 (Maghemite)
650	2	None
650	2×10^{-1}	γ-Fe_2O_3 (Maghemite)
650	5×10^{-2}	γ-Fe_2O_3 (Maghemite)

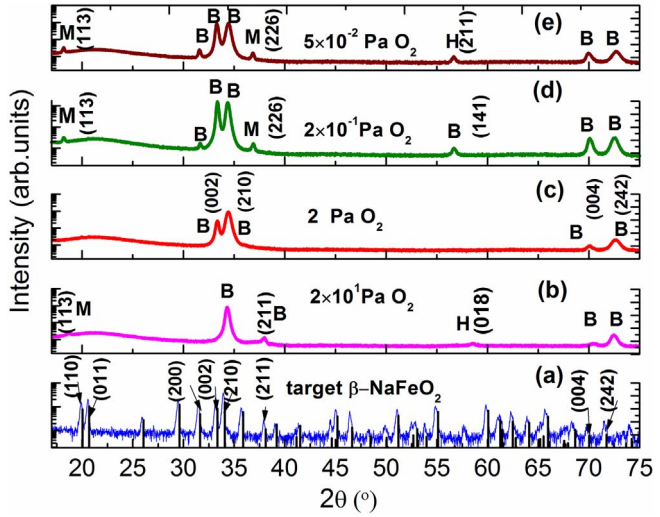

Fig. 4. X-ray diffraction patterns of β-$NaFeO_2$ thin films obtained from a polycrystalline target (a) under different oxygen partial pressures. The partial oxygen pressure 2 Pa has resulted in the growth of a pure β-$NaFeO_2$ thin film (c) whereas under the pressures of 2×10 Pa (b), 2×10^{-1} Pa (d) and 5×10^{-2} Pa (e) thin films of β-$NaFeO_2$ with secondary phases have been produced.

structure has a highly anisotropic character along the c-axis, as observed for example in $CuCrO_2$ thin films prepared by sol-gel [39] or chemical solution deposition [10] methods, the (00l) reflection does not seem to have a dominant role in the β-$NaFeO_2$ thin films. The weak character of the (00l) reflection has also been reported for the $CuCrO_2$ thin films prepared by radio frequency (RF) sputtering and is believed to be correlated with the oxygen stoichiometry [9].

The parameter, that proved to be very critical for the formation of pure single phase thin film of β-$NaFeO_2$, is the partial O_2 pressure, as it has been observed also in the case of $BiFeO_3$ thin films [48] prepared by PLD. The growth conditions of pure β-$NaFeO_2$ thin films and the films with secondary phases are summarized in Table 1. At 2 Pa, pure β-$NaFeO_2$ can be fabricated. Fig. 4 shows the presence of iron oxides as impurity phases depending on the variation of the partial oxygen pressure that was utilised during the β-$NaFeO_2$ thin film growth. Reflections from two iron oxides have been observed as parasitic phases, namely: the α-Fe_2O_3 (hematite) and the Fe_2O_3 (maghemite). The Bragg reflections attributed to iron oxides are marked in Fig. 4 with the letter H and M, for the hematite (ISCD 43465) and maghemite (ICSD 87119), respectively. The relevant hkl indices are also indicated in panels (a) and (c) for the β-$NaFeO_2$ target and thin film, respectively, whereas in the rest of the panels for the hkl of the secondary phases are also shown. Since the growth of β-$NaFeO_2$ thin films is observed only for the oxygen pressures at 2 Pa it becomes clear that the formation of the pure phase from this delafossite depends primarily on the partial oxygen pressure and that deviations from this pressure result in the presence of secondary phases.

Fig. 5 depicts the surface morphology of the single phase β-$NaFeO_2$ thin films, for different magnifications. In Fig. 5(a) it is shown that the surface of the films is uniform over large areas, and it comprises of a flat areas onto which islands of lamellar, flower-like structures are grown. Images in higher magnifications in Fig. 5(b), (c) and (d) show in greater detail the two domains of the film. Specifically, the lamellar flower-like part is shown in detail in Fig. 5(c) while the flat part is shown in Fig. 5(d). Similar flower like structures have also been observed in iron oxide nanoparticles [49]. AFM confirms the structure, as shown in Fig. 6(a) and (b). Both images were obtained from different films prepared under the same PLD conditions. One morphological difference

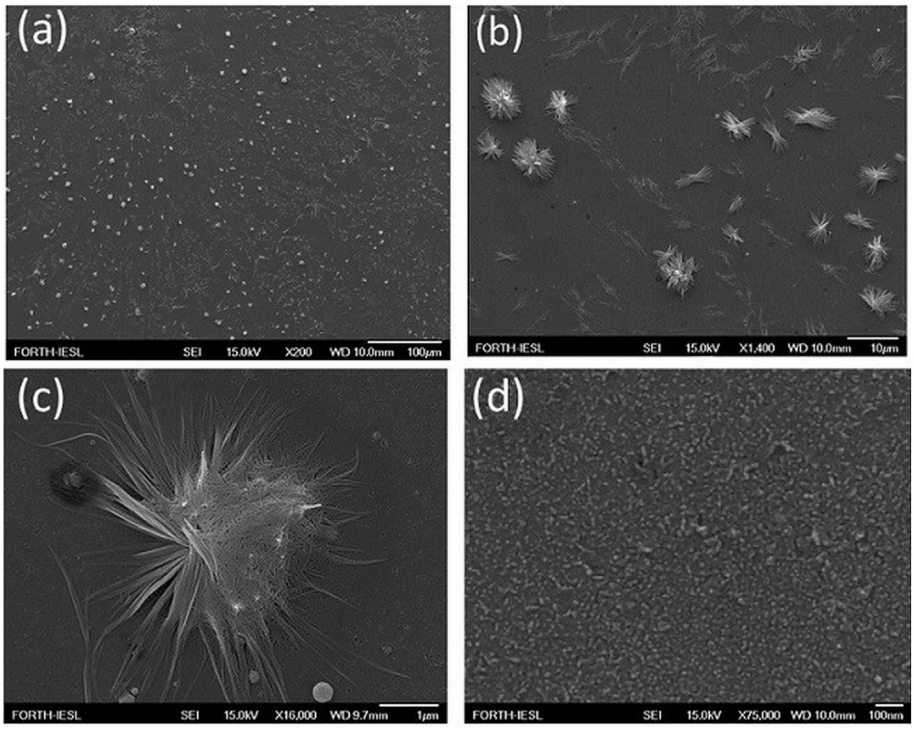

Fig. 5. SEM topography of β-$NaFeO_2$ thin films obtained by various magnifications (a) at 100 μm, (b) at 10 μm, (c) at 1 μm and (d) at 100 nm.

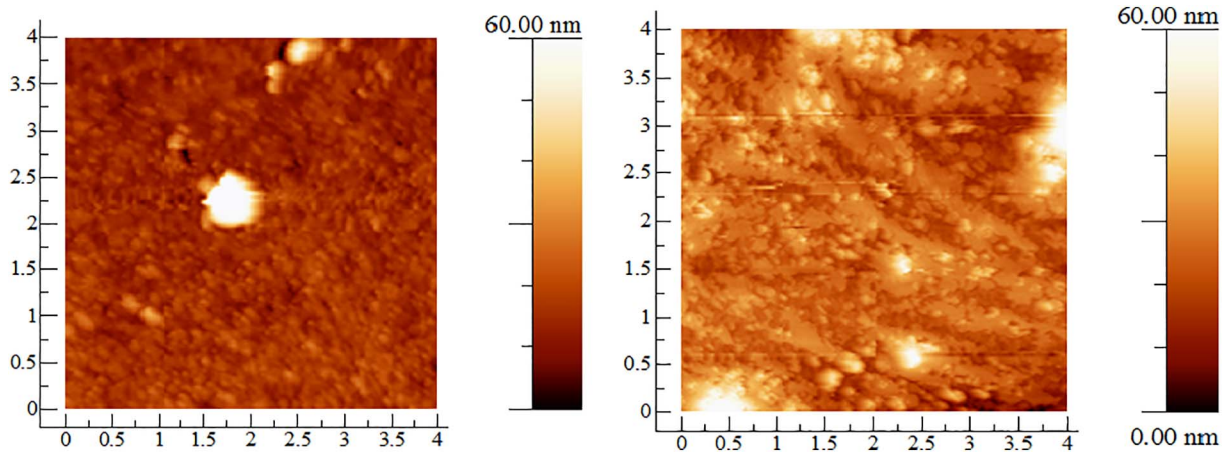

Fig. 6. 4 × 4 μm^2 Atomic Force Microscopy (AFM) images of β-$NaFeO_2$ films support 2D growth.

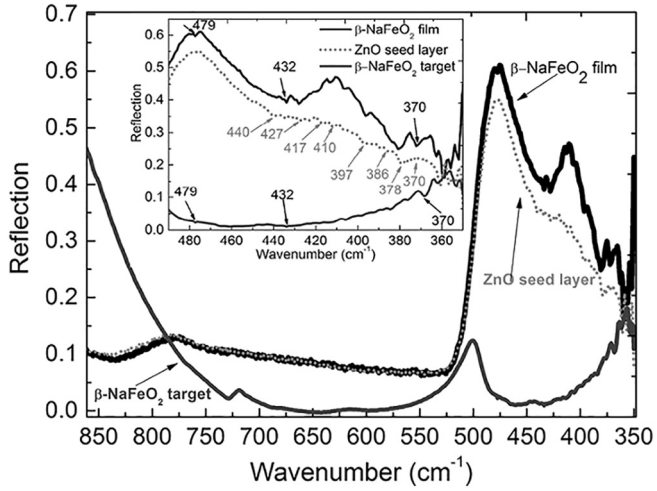

Fig. 7. FT-IR spectra of the β-$NaFeO_2$ pollycrystalline target, the ZnO seed layer and the β-$NaFeO_2$ thin film, shown with the dark gray, dashed light gray and black lines. The bands at about 479 cm^{-1} and 432 cm^{-1} and 370 cm^{-1} are the characteristic bands of β-$NaFeO_2$ formation.

Table 2
The characteristic bands and the corresponding types of vibrations for the β-$NaFeO_2$ powder and thin films and the substrate ZnO, as shown in Fig. 6.

Vibration wavenumber (cm^{-1})	Material	Corresponding vibration
479	β-$NaFeO_2$ target	Mixed stretching-bending modes of FeO_4 tetrahedra
434	β-$NaFeO_2$ target	
428	β-$NaFeO_2$ target	
440	ZnO	ZnO stretching modes
427	ZnO	
417	ZnO	
410	ZnO	
397	ZnO	
386	ZnO	
378	ZnO	
370	ZnO	
432	β-$NaFeO_2$ thin film	Mixed stretching-bending modes of FeO_4 tetrahedra
370	β-$NaFeO_2$ thin film	

observed in two different areas of the same film is shown in Fig. 6(a) and (b). Fig. 6(a) shows that an area of the film consists of granules at the nm scale, whereas Fig. 6(b) shows features of a laminar morphology, which is probably related to the flower-like structures observed by the SEM in Fig. 5(c). The root mean square (RMS) roughness varies from 4 nm to 8 nm in the xy scale of our experiments revealing a smooth surface that supports two dimensional growth. These values of RMS are quite higher than the ones reported for as deposited $CuCrO_2$ samples (RMS = 0.4 nm). However a direct comparison of the morphology obtained by various delafossite films is quite challenging. The preparation conditions and the annealing treatment should be taken into account, as it has been observed in topography studies of $CuFeO_2$ [25] and $CuCrO_2$ [9,50] obtained by sputtering. For example the RMS varies from 3.6 nm for the case of the amorphous $CuCrO_2$ to 17 nm for a single phase, high temperature annealed $CuCrO_2$ thin film [50].

FT-IR measurements were performed in order to verify the purity of the as-grown β-$NaFeO_2$ films and the possible existence of characteristic bands, attributed to different crystal structures of iron oxides, such as hematite and maghemite. The FT-IR spectra were carried out in reflection mode in the range of 350–8500 cm^{-1}. Spectra were obtained from the ZnO seed layer, the β-$NaFeO_2$ polycrystalline target and the thin films of β-$NaFeO_2$, represented in Fig. 7 with gray, dark gray and black lines, respectively. The resolved vibrational bands were identified and appended in Table 2. The FT-IR spectra of the β-$NaFeO_2$ pollycrystalline target (black line in Fig. 7), reveal three characteristic reflection bands which are common to pure β-$NaFeO_2$ and its solid solutions, namely, 728 cm^{-1}, 479 cm^{-1} and 432 cm^{-1} attributed to FeO_4 tetrahedra [51]. The comparison of the reflection spectra that correspond to ZnO and β-$NaFeO_2$ films grown on ZnO layers, reveals several characteristic peaks centered (marked with arrows in the inset of Fig. 7) at ~440 cm^{-1}, ~427 cm^{-1}, ~417 cm^{-1}, ~410 cm^{-1}, ~397 cm^{-1}, ~386 cm^{-1}, ~378 cm^{-1}, and ~370 cm^{-1} which are attributed to vibrations of ZnO bonds, in agreement with previous literature reports [52–54]. Moreover, two clear reflection bands (already resolved from the β-$NaFeO_2$ pollycrystalline target) at about 370 cm^{-1} and 432 cm^{-1}, appear only for the case of β-$NaFeO_2$ films and are shown in the inset of Fig. 7. These are the characteristic bands of β-$NaFeO_2$, as already discussed by Rulmont et al. [51], indicating that ZnO is indeed a suitable substrate in order to grow β-$NaFeO_2$ films.

4. Conclusions

We have grown the beta phase of the sodium iron oxide with the delafossite structure in thin film. The preparation of the β-$NaFeO_2$ thin films on ZnO seed layers was achieved by pulsed laser deposition using β-$NaFeO_2$ polycrystalline powders. The growth of β-$NaFeO_2$ is strongly favored at 600 °C at an oxygen partial pressure of 2 Pa. Pressure

deviations by 10 Pa resulted in the appearance of iron oxides as secondary phases. Specifically higher oxygen pressure resulted in the appearance of hematite and maghemite, whereas lower partial oxygen pressures (10^{-1}–10^{-2} Pa) led to the formation of maghemite. The thin films have been characterized by X-ray diffraction confirming that the pure phase of β-$NaFeO_2$ has been obtained. AFM topography confirms a two dimensional growth, whereas FT-IR measurements reveal reflection bands characteristic for the deposited phase.

Acknowledgements

This research has been in part carried out in the framework of the Heracleitus II project (Grant No.349309.WP1.56) co-financed by the Ministry of Education & Religious Affairs, Greece and the European Social Fund, European Union (Operational Program "Education and Lifelong Learning" of the 'National Strategic Reference Framework, NSRF, 2007–2013). The PLD experimental work was conducted at the Ultraviolet Laser Facility at FORTH-IESL, supported in part by the European Union's Horizon 2020 research and innovation programme LASERLAB-EUROPE (Grant Agreement No. 654148. We would also like to thank Mrs. Aleka Manousaki for her help with the SEM experiments.

References

[1] A. Buljan, P. Alemany, E. Ruiz, Electronic structure and bonding in CuMO2 (M = Al, Ga, Y) Delafossite-type oxides: an ab initio study, J. Phys. Chem. B 103 (1999) 8060–8066.
[2] A. Zorko, O. Adamopoulos, M. Komelj, D. Arčon, A. Lappas, Frustration-induced nanometre-scale inhomogeneity in a triangular antiferromagnet, Nat. Commun. 5 (2014) 3222.
[3] B. Kundys, A. Maignan, D. Pelloquin, C. Simon, Magnetoelectric interactions in polycrystalline multiferroic antiferromagnets CuFe1-xRhxO2 (x = 0.00 and x = 0.05), Solid State Sci. 11 (2009) 1035–1039.
[4] Y. Takeda, K. Nakahara, M. Nishijima, N. Imanishi, O. Yamamoto, M. Takano, R. Kanno, Sodium deintercalation from sodium iron oxide, Mater. Res. Bull. 29 (1994) 659–666.
[5] A.M. Sukeshini, H. Kobayashi, M. Tabuchi, H. Kageyama, Physicochemical characterization of $CuFeO_2$ and lithium intercalation, Solid State Ionics 128 (2000) 33–41.
[6] A.R. Armstrong, P.G. Bruce, Synthesis of layered LiMnO2 as an electrode for rechargeable lithium batteries, Nature 381 (1996) 499–500.
[7] I. Kruk, P. Zajdel, W. van Beek, I. Bakaimi, A. Lappas, C. Stock, M.A. Green, Coupled commensurate cation and charge modulation in the tunneled structure, Na0.40(2) MnO2, J. Am. Chem. Soc. 133 (2011) 13950–13956.
[8] H. Kawazoe, M. Yasukawa, H. Hyodo, M. Kurita, H. Yanagi, H. Hosono, P-type electrical conduction in transparent thin films of $CuAlO_2$, Nature 389 (1997) 939–942.
[9] A. Barnabe, Y. Thimont, M. Lalanne, L. Presmanes, P. Tailhades, p-Type conducting transparent characteristics of delafossite Mg-doped CuCrO2 thin films prepared by RF-sputtering, J. Mater. Chem. C 3 (2015) 6012–6024.
[10] T.-W. Chiu, S.-W. Tsai, Y.-P. Wang, K.-H. Hsu, Preparation of p-type conductive transparent CuCrO2:Mg thin films by chemical solution deposition with two-step annealing, Ceram. Int. 38 (Suppl. 1) (2012) S673–S676.
[11] O. Yasuhiro, S. Ken-ichi, N. Tomohiro, K. Tsuyoshi, Structural, magnetic and thermoelectric properties of delafossite-type oxide, $CuCr_{1-x}Mg_xO_2$ ($0 \le x \le 0.05$), Jpn. J. Appl. Phys. 46 (2007) 1071.
[12] X. Wang, Z. Shi, S. Yao, F. Liao, J. Ding, M. Shao, Gamma ray irradiated $AgFeO_2$ nanoparticles with enhanced gas sensor properties, J. Solid State Chem. 219 (2014) 228–231.
[13] N. Terada, D.D. Khalyavin, P. Manuel, Y. Tsujimoto, K. Knight, P.G. Radaelli, H.S. Suzuki, H. Kitazawa, Spiral-spin-driven ferroelectricity in a multiferroic delafossite $AgFeO_2$, Phys. Rev. Lett. 109 (2012) 097203.
[14] A. Maignan, C. Martin, K. Singh, C. Simon, O.I. Lebedev, S. Turner, From spin induced ferroelectricity to dipolar glasses: spinel chromites and mixed delafossites, J. Solid State Chem. 195 (2012) 41–49.
[15] M.O. Sullivan, P. Stamenov, J. Alaria, M. Venkatesan, J.M.D. Coey, Magnetoresistance of $CuCrO_2$-based delafossite films, J. Phys. Conf. Ser. 200 (2010) 052021.
[16] S. Seki, Y. Onose, Y. Tokura, Spin-driven ferroelectricity in triangular lattice Antiferromagnets $ACrO_2$ (a = cu, ag, li, or Na), Phys. Rev. Lett. 101 (2008) 067204.
[17] D.I. Khomskii, Multiferroics: different ways to combine magnetism and ferroelectricity, J. Magn. Magn. Mater. 306 (2006) 1–8.
[18] N.A. Hill, Why are there so few magnetic ferroelectrics? J. Phys. Chem. B 104 (2000) 6694–6709.
[19] T. Zhao, A. Scholl, F. Zavaliche, K. Lee, M. Barry, A. Doran, M.P. Cruz, Y.H. Chu, C. Ederer, N.A. Spaldin, R.R. Das, D.M. Kim, S.H. Baek, C.B. Eom, R. Ramesh, Electrical control of antiferromagnetic domains in multiferroic $BiFeO_3$ films at room temperature, Nat. Mater. 5 (2006) 823–829.
[20] H. Zheng, J. Wang, S.E. Lofland, Z. Ma, L. Mohaddes-Ardabili, T. Zhao, L. Salamanca-Riba, S.R. Shinde, S.B. Ogale, F. Bai, D. Viehland, Y. Jia, D.G. Schlom, M. Wuttig, A. Roytburd, R. Ramesh, Multiferroic $BaTiO_3$-$CoFe_2O_4$ Nanostructures, Science 303 (2004) 661–663.
[21] H. Watanabe, M. Fukase, Weak ferromagnetism in β-$NaFeO_2$, J. Phys. Soc. Jpn. 16 (1961) 1181–1184.
[22] M. Viret, D. Rubi, D. Colson, D. Lebeugle, A. Forget, P. Bonville, G. Dhalenne, R. Saint-Martin, G. André, F. Ott, β-$NaFeO_2$, a new room-temperature multiferroic material, Mater. Res. Bull. 47 (2012) 2294–2298.
[23] J. Wang, J.B. Neaton, H. Zheng, V. Nagarajan, S.B. Ogale, B. Liu, D. Viehland, V. Vaithyanathan, D.G. Schlom, U.V. Waghmare, N.A. Spaldin, K.M. Rabe, M. Wuttig, R. Ramesh, Epitaxial $BiFeO_3$ multiferroic thin film heterostructures, Science 299 (2003) 1719.
[24] R.V. Wang, D.D. Fong, F. Jiang, M.J. Highland, P.H. Fuoss, C. Thompson, A.M. Kolpak, J.A. Eastman, S.K. Streiffer, A.M. Rappe, G.B. Stephenson, Reversible chemical switching of a ferroelectric film, Phys. Rev. Lett. 102 (2009) 047601.
[25] A. Barnabé, E. Mugnier, L. Presmanes, P. Tailhades, Preparation of delafossite $CuFeO_2$ thin films by rf-sputtering on conventional glass substrate, Mater. Lett. 60 (2006) 3468–3470.
[26] H.-Y. Chen, W.-J. Yang, K.-P. Chang, Characterization of delafossite-$CuCrO_2$ thin films prepared by post-annealing using an atmospheric pressure plasma torch, Appl. Surf. Sci. 258 (2012) 8775–8779.
[27] V.C. Alan, N.B. Aran, R. Aline, Y. Cedric, A structural study of delafossite-type $CuInO_2$ thin films, J. Phys. Conf. Ser. 249 (2010) 012045.
[28] F. Liu, T. Makino, H. Hiraga, T. Fukumura, Y. Kong, M. Kawasaki, Ultrafast dynamics of excitons in delafossite $CuScO_2$ thin films, Appl. Phys. Lett. 96 (2010) 211904.
[29] J. Ding, Y. Sui, W. Fu, H. Yang, S. Liu, Y. Zeng, W. Zhao, P. Sun, J. Guo, H. Chen, M. Li, Synthesis and photoelectric characterization of delafossite conducting oxides $CuAlO_2$ laminar crystal thin films via sol-gel method, Appl. Surf. Sci. 256 (2010) 6441–6446.
[30] V.R. Palkar, K. Prashanthi, S.P. Dattagupta, Influence of process-induced stress on multiferroic properties of pulse laser deposited Bi 0.7 Dy 0.3 FeO_3 thin films, J. Phys. D. Appl. Phys. 41 (2008) 045003.
[31] S.Z. Li, J. Liu, X.Z. Wang, B.W. Yan, H. Li, J.M. Liu, Epitaxial growth of delafossite $CuFeO_2$ thin films by pulse laser deposition, Phys. B Condens. Matter 407 (2012) 2412–2415.
[32] A.M. Abakumov, A.A. Tsirlin, I. Bakaimi, G. Van Tendeloo, A. Lappas, Multiple twinning as a structure directing mechanism in layered rock-salt-type oxides: $NaMnO_2$ polymorphism, redox potentials, and magnetism, Chem. Mater. 26 (2014) 3306–3315.
[33] L.R. Cox, E.H. Dunlop, A.M. North, $NaAlO_2$ and $NaFeO_2$ polymorpshism, Nature 249 (1974) 245.
[34] Y. Takeda, J. Akagi, A. Edagawa, M. Inagaki, S. Naka, A preparation and polymorphic relations of sodium iron oxide (NaFeO2), Mater. Res. Bull. 15 (1980) 1167–1172.
[35] T. Joshi, T.R. Senty, R. Trappen, J. Zhou, S. Chen, P. Ferrari, P. Borisov, X. Song, M.B. Holcomb, A.D. Bristow, A.L. Cabrera, D. Lederman, Structural and magnetic properties of epitaxial delafossite $CuFeO_2$ thin films grown by pulsed laser deposition, J. Appl. Phys. 117 (2015) 013908.
[36] K. Ueda, T. Hase, H. Yanagi, H. Kawazoe, H. Hosono, H. Ohta, M. Orita, M. Hirano, Epitaxial growth of transparent p-type conducting $CuGaO_2$ thin films on sapphire (001) substrates by pulsed laser deposition, J. Appl. Phys. 89 (2001) 1790–1793.
[37] E. Mugnier, A. Barnabé, L. Presmanes, P. Tailhades, Thin films preparation by rf-sputtering of copper/iron ceramic targets with Cu/Fe = 1: from nanocomposites to delafossite compounds, Thin Solid Films 516 (2008) 1453–1456.
[38] A.N. Banerjee, R. Maity, K.K. Chattopadhyay, Preparation of p-type transparent conducting $CuAlO_2$ thin films by reactive DC sputtering, Mater. Lett. 58 (2004) 10–13.
[39] S. Götzendörfer, R. Bywalez, P. Löbmann, Preparation of p-type conducting transparent $CuCrO_2$ and $CuAl0.5Cr0.5O_2$ thin films by sol-gel processing, J. Sol-Gel Sci. Technol. 52 (2009) 113–119.
[40] S. Götzendörfer, C. Polenzky, S. Ulrich, P. Löbmann, Preparation of CuAlO2 and $CuCrO_2$ thin films by sol-gel processing, Thin Solid Films 518 (2009) 1153–1156.
[41] F. Mao, T. Nyberg, T. Thersleff, A.M. Andersson, U. Jansson, Combinatorial magnetron sputtering of $AgFeO_2$ thin films with the delafossite structure, Mater. Des. 91 (2016) 132–142.
[42] I.E. Grey, R.J.H.A.W. Hewat, A neutron powder diffraction study of the β to γ phase transformation in $NaFeO_2$, Zeitschrift für Kristallographie, 1990, p. 51.
[43] E.L. Papadopoulou, M. Varda, A. Pennos, M. Kaloudis, M. Kayambaki, M. Androulidaki, K. Tsagaraki, Z. Viskadourakis, O. Durand, G. Huyberechts, E. Aperathitis, The effect of PLD deposition parameters on the properties of p-$SrCu_2O_2$/n-Si diodes, Thin Solid Films 516 (2008) 8154–8158.
[44] I. Horcas, R. Fernández, J.M. Gómez-Rodríguez, J. Colchero, J. Gómez-Herrero, A.M. Baro, WSXM: a software for scanning probe microscopy and a tool for nanotechnology, Rev. Sci. Instrum. 78 (2007) 013705.
[45] J. Rodríguez-Carvajal, Recent advances in magnetic structure determination by neutron powder diffraction, Phys. B Condens. Matter 192 (1993) 55–69.
[46] F. Bertaut, P. Blum, Structure d'une nouvelle variete de ferrited de sodium(Fe Na O_2), C. R. Hebd. Seances Acad. Sci. 239 (1954) 429–431.
[47] Y.-N. Xu, W.Y. Ching, Electronic, optical, and structural properties of some wurtzite crystals, Phys. Rev. B 48 (1993) 4335–4351.
[48] H. Béa, M. Bibes, A. Barthélémy, K. Bouzehouane, E. Jacquet, A. Khodan, J.-P. Contour, S. Fusil, F. Wyczisk, A. Forget, D. Lebeugle, D. Colson, M. Viret, Influence of parasitic phases on the properties of $BiFeO_3$ epitaxial thin films, Appl. Phys. Lett. 87 (2005) 072508.

[49] F.N. Sayed, V. Polshettiwar, Facile and sustainable synthesis of shaped iron oxide nanoparticles: effect of iron precursor salts on the shapes of iron oxides, Sci. Rep. 5 (2015) 9733.
[50] R.-S. Yu, C.-M. Wu, Characteristics of p-type transparent conductive $CuCrO_2$ thin films, Appl. Surf. Sci. 282 (2013) 92–97.
[51] A. Rulmont, P. Tarte, J.M. Winand, M. Almou, (β-NaFeO2)1-x(SiO2, GeO2)x solid solutions: a study by X-ray diffraction, IR spectroscopy, and ionic conductivity measurements, J. Solid State Chem. 97 (1992) 156–162.
[52] S. Musić, M. Dragčević, S. Popović Maljković, Influence of chemical synthesis on the crystallization and properties of zinc oxide, Mater. Chem. Phys. 77 (2003) 521–530.
[53] D. Vernardou, G. Kenanakis, S. Couris, A.C. Manikas, G.A. Voyiatzis, M.E. Pemble, E. Koudoumas, N. Katsarakis, The effect of growth time on the morphology of ZnO structures deposited on Si (100) by the aqueous chemical growth technique, J. Cryst. Growth 308 (2007) 105–109.
[54] S. Hayashi, N. Nobuyuki, K. Hitoshi, Generalized theory of average dielectric constant and its application to infrared absorption by ZnO small particles, J. Phys. Soc. Jpn. 46 (1979) 176–183.